Hysteresis self-bearing motor

Mohammad Imani-Nejad[a], David L. Trumper[b]

[a] Massachusetts Institute of Technology , 77 Massachusetts ave, Cambridge, USA, m_imani@alum.mit.edu
[b] Massachusetts Institute of Technology , 77 Massachusetts ave, Cambridge, USA, trumper@mit.edu

***Abstract*—This paper presents a hysteresis self-bearing motor along with its nonlinear analysis. In this work we introduced a new type of self-bearing motor with segmented stator. The major advantages of this stator are: easy and low cost manufacturing, higher filling factor and shorter magnetic path for the stator. We tested the self-bearing concept successfully with this new configuration. Hysteresis motors are suitable for high speed application since their rotor has neither permanent magnets nor any winding or mechanical features. We used FEA analysis to check the feasibility of proposed idea. Then we used Chua's hysteresis model to simulate the nonlinear behavior of this system.**

***Index Terms*—Self-bearing motor, Axial flux, Hysteresis, Chua, Segmented.**

I. Introduction

Many types of self-bearing motors have been presented in the literature. Permanent magnet self-bearing motors are widely proposed for a variety of applications; however they have some disadvantages for high speed and high temperature systems. Induction self-bearing motors have been proposed since at least early 1990 [1] and [2]. For an output of more than a few kilowatts, induction machines are competitive to permanent magnet motors. They are also less expensive and more robust compared to PM machines.

Hysteresis motors are a synchronous induction machine. Steinmetz apparently introduced the first hysteresis motor in 1917, as stated in [3]. This type of motor has a simple solid rotor of material with large magnetic hysteresis. They also typically have a polyphase stator winding similar to an induction machine. Like induction machines, a slotted stator having distributed windings is used to produce as nearly as possible a sinusoidal magnetic flux distributed spatially. The rotating magnetic field creates magnetic poles in the rotor by means of induction. These poles follow the stator magnetic field. Because of hysteresis, the rotor poles lag behind the inducing magneto motive force wave by the hysteretic lag angle. Before the rotor reaches synchronous speed, a given region of the rotor experiences a cyclic hysteresis loop at the slip frequency. Under this circumstance, the lag angle is only a function of the rotor material, and it remains at its maximum value. When the rotor reaches synchronous speed with an initial load, due to the rotor inertia interacting with magnetic stiffness, the lag angle starts to oscillate about its equilibrium point until the hysteresis torque is sufficient to carry the load. Typically the period of these oscillations is about 1-5 seconds. This phenomena is called hunting.

On the other hand different types of multiple winding structure have been presented in the literature. This type of machines have suspension windings in addition to motor windings. Typically, by controlling current through a combination of P pole and P$\pm$2 pole windings the rotor is levitated and rotated. One of the main disadvantages of such a system, especially for axial type motors is the low filling factor for the stator. This is a practical issue because winding of such a stator is not an easy task. On the contrary, U core actuators have a very good filling factor. Moreover, these type of actuators are much easier to manufacture and less expensive compared to conventional axial stators. Another advantage of a segmented stator is the short magnetic path in the stator. In this paper we present a segmented stator design for hysteresis self-bearing motor along with non-linear analysis.

II. Principle of Operation

A. Configuration

The primary goal of designing this system is introducing a new self-bearing motor for high speed flywheels. High speed flywheel rotors experience large expansion due to high centrifugal force. This causes large gap variation in radial flux motors. Thus we chose an axial flux type self-bearing motor where the expansion occurs in the non-sensitive direction.

Figure 1 shows the fabricated prototype of segmented stator and hysteretic rotor. The complete setup has two stators: one on the top and one on the bottom for torque control. In our experimental setup we used 12 U cores of laminated silicon iron to build the segmented stator. The rotor is fabricated from D2 tool steel. This configuration enables us to implement either a two or a four pole motor simply by changing the current pattern.

B. Magnetic flux distribution

It is very important to explain how the magnetic path is formed in the rotor in the first place. Even though a simple solid ring would work in this design, instead we propose a composite ring such as shown in figure 2.

As we can see in this figure, the gap between the two rings causes a circumferential magnetic field in both rings. We used epoxy to fill this gap, however for real application this gap can be filled with composite material such as carbon fibre. This is an advantage for high speed systems, where we can use high hysteresis material for the rings and over wrap it with a strong material such as carbon fiber. In this case, steels with large density provide the mass whereas the carbon fibre gives

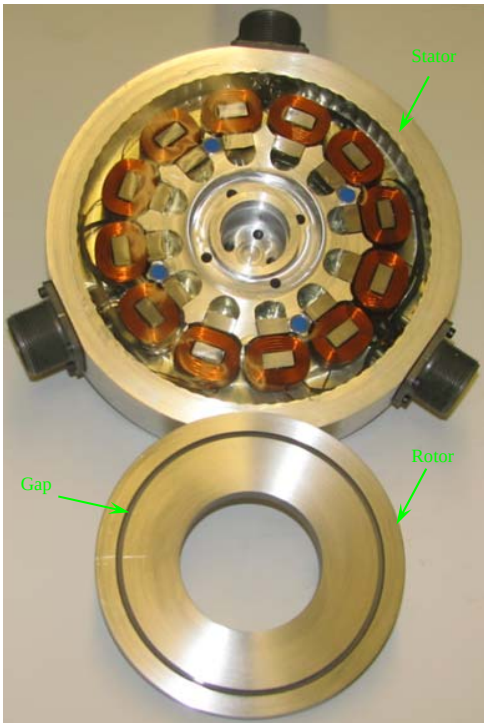

Fig. 1. Hysteresis self-bearing motor. The rotor ring is levitated and rotated by a hysteresis motor structure.

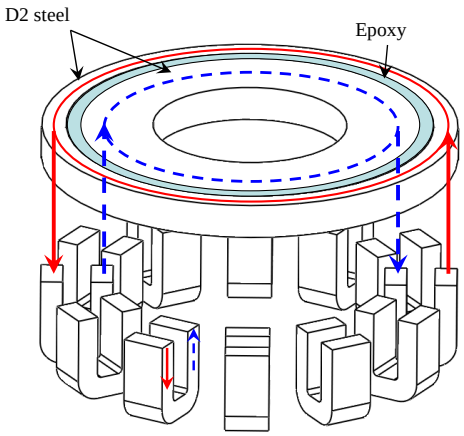

Fig. 2. Segmented stator-rotor magnetic path in composite ring rotor.

the strength to the rotor structure. The other advantage of the segmented stator configuration which can be seen in figure 2 is that the magnetic path in the stator is relatively short.

Figure 3 shows an FEA simulation for the two pole motor configuration. The FEA analysis shows that magnetic in the rotor is similar to that generated in the regular stator.

C. Control

Figure 4 shows the control block diagram for our system.

As shown in this figure there are three control loops for levitation control ,i.e., the x and the two tip tilt θ_z and θ_y axes. The commutated signals are added and subtracted to the upper and lower stator respectively. The torque is controlled

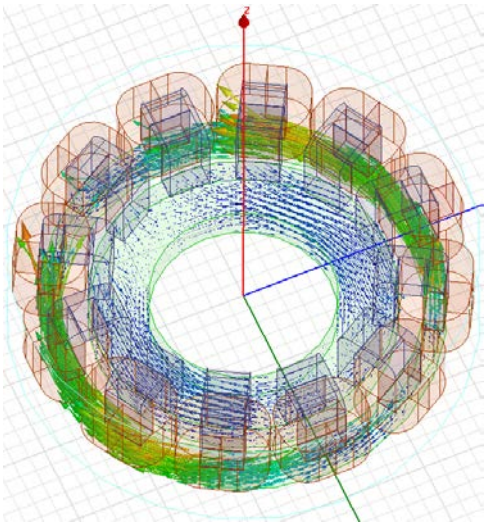

Fig. 3. FEA simulation for segmented stator in two pole configuration.

by a bias current that is shown by T. This bias current is added differentially to top and lower stator; thus it enables us to vary the shear magnetic field. Since the hysteresis motor can run synchronous, we can simply use a $\frac{V}{f}$ control strategy for speed regulation. However we can also run the system with a closed loop velocity control as needed.

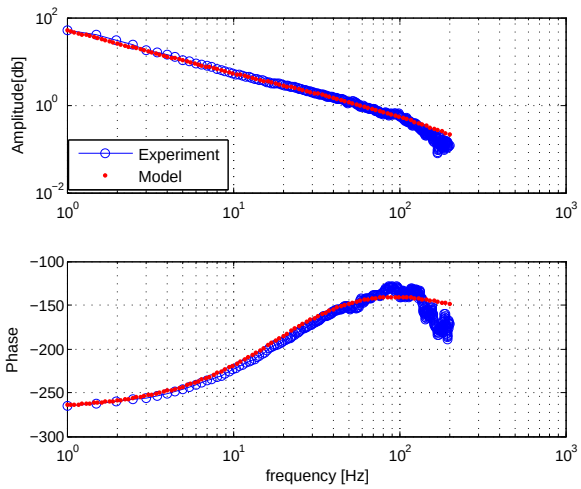

Fig. 5. Loop transfer function frequency response for axial direction. Cross over frequency is $f_c = 60$Hz with phase margin $\phi_m = 40°$

A lead-lag controller is designed for a cross over frequency of $f_c = 60$Hz and phase margin of $\phi_m = 40°$ which provides approximately $\zeta = 0.4$ damping. The loop transfer function frequency responses for both vertical and tilting axes are given in Figures 5 and 6.

As we can see in figure 6, the tip tilt phase differs significantly from theory at low frequencies. We believe that this is due to lateral mode coupling. Since the rotor is passively stable in lateral axes thus it can couple with a lateral mode. We can also see a resonance at 200Hz which is a structural resonance.

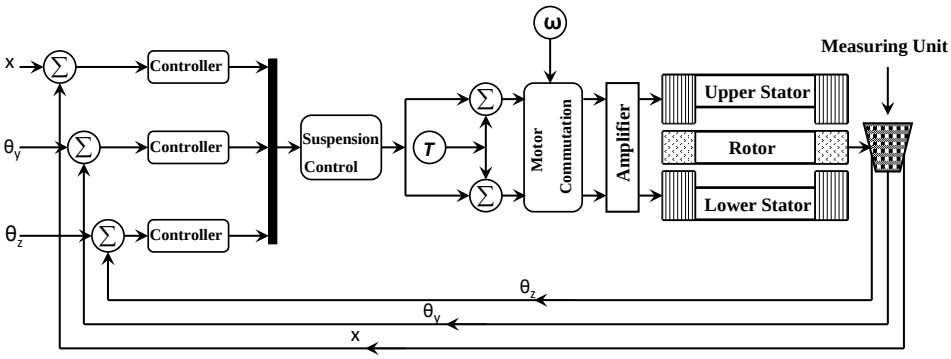

Fig. 4. Single winding self-bearing control block diagram.

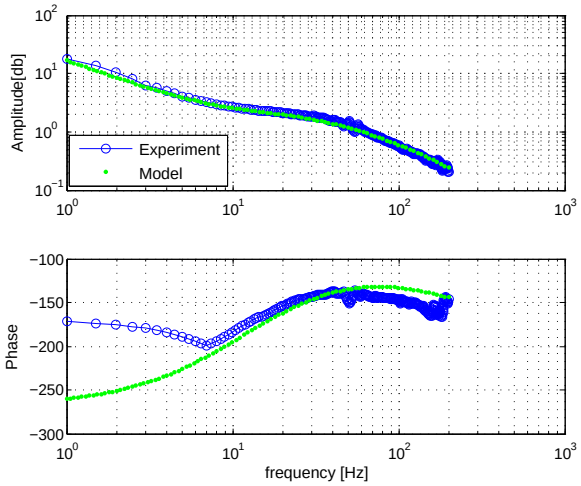

Fig. 6. Loop transfer function frequency response for tip/tilt direction (θ).

III. Non-linear Analysis

A. Chua Hysteresis Model

In this analysis we use a Chua nonlinear hysteresis model [4]. The Chua hysteresis model is given by

$$\frac{dy(t)}{dt} = W\left(\frac{dx(t)}{dt}\right) \times h\left(y(t)\right) \times g\left[x(t) - f(y(t))\right]. \quad (1)$$

In this equation $x(t)$ is the input and $y(t)$ is the output. The model is specified by two monotonically increasing functions: f the *restoring function* which describes the energy storage, and g, the *dissipation function* which describes the energy dissipation. The W and h functions provide the loop widening and weighting functions respectively. These four functions should be tuned such that the desired hysteresis loop is attained. Chua and Bass have illustrated the hysteresis loop for two different types of material in [5]. In this paper they also present several possible functions for loop widening.

As an example, functions f and g were replaced by the logarithmic functions given below to simulate the D2 steel hysteresis loop shown in figure 7. We chose absolute function for W and unity gain for h.

$$\begin{aligned} f(y) &= \frac{\text{sign(y)}}{-0.005} \ln\left[1 - \frac{1}{0.7}|y|\right] \\ g(u) &= -50 \ln\left[1 - \frac{1}{1500}|u|\right] \end{aligned} \quad (2)$$

The B-H curve used in this analysis is the Chua's model fitted for D2 steel shown in figure 8.

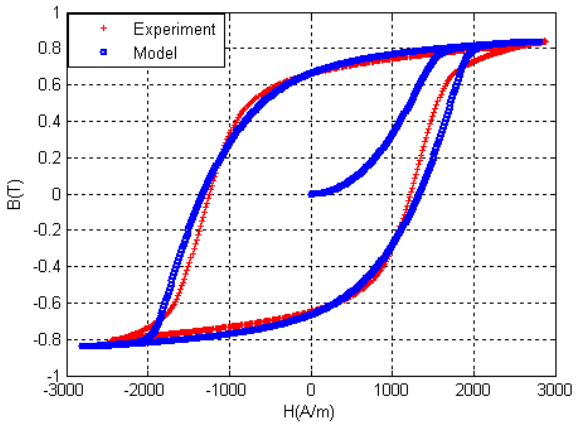

Fig. 8. Hysteresis model of Chua's configuration as fitted to D2 steel experimental data.

B. Suspension Forces and Moments

In this section we present the analysis of suspension forces and moments for hysteresis self-bearing motors.

We derive the governing equations and present the SIMULINK block diagram for axial force. A similar analysis can be easily used for inclination moments. For this purpose we only need to replace the force, displacement and mass by moment, inclination, and moment of inertia, respectively.

Figure 9 shows the magnetic path for a U core actuator and a segment of the rotor. In case of homogenous magnetic field the magnetic normal stress σ is given:

$$\sigma = \frac{B^2}{2\mu_0}. \quad (3)$$

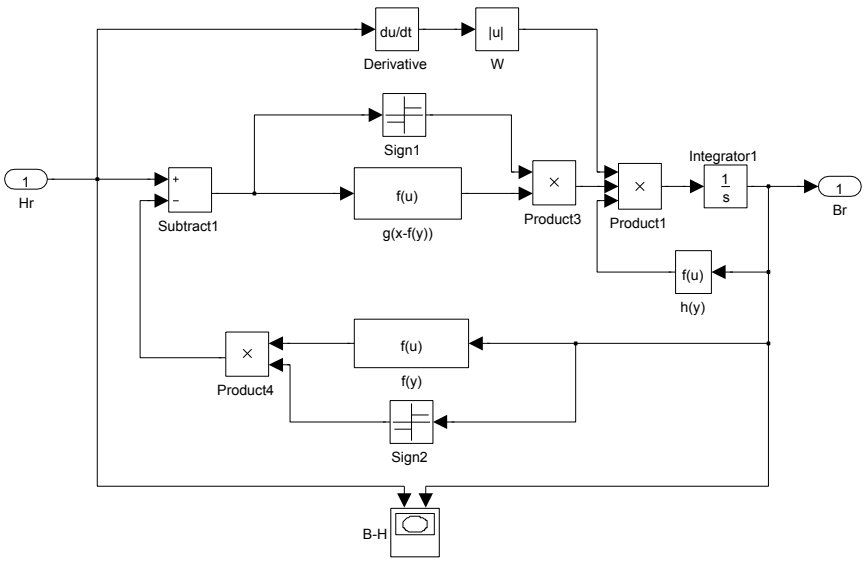

Fig. 7. Chua model Simulink block diagram.

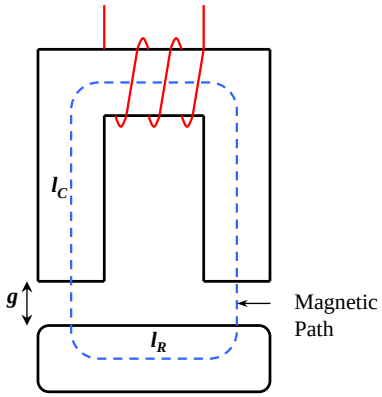

Fig. 9. Magnetic path for U core actuator.

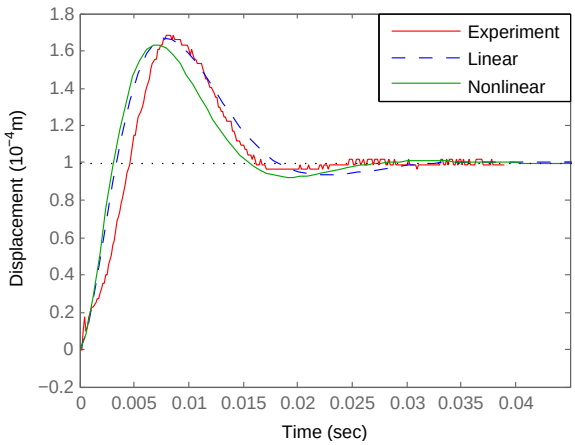

Fig. 12. Step response. Zero reference corresponds to a gap of 0.5mm.

Therefore the force is given by:

$$f = A\frac{B^2}{2\mu_0}; \tag{4}$$

where A is the active surface area of the electromagnet. Meanwhile we can write Ampere's law along the magnetic path

$$Ni = H_R l_R + H_g l_g + H_c l_c, \tag{5}$$

where l_R, l_g and l_c are the length of magnetic paths in rotor, gap and stator respectively. In this analysis we assume that the stator permeability is much larger than the air and the rotor. Thus we can write:

$$H_R = \frac{(Ni - H_g l_g)}{l_R}. \tag{6}$$

Figure 10 shows the block diagram of force generation. The block is constructed based on the equations presented above. The block has two inputs: current and displacement (inclination). The magnetic field intensity H_R for the rotor is calculated by using (6). The magnetic flux density is then computed through Chua's model. For homogenous magnetic flux density and ignoring fringes, the magnetic flux density is constant i.e. $B_g = B_R$. Thus we can calculate the magnetic field intensity in gap by:

$$H_g = \frac{B_g}{\mu_0}. \tag{7}$$

Once we have the magnetic field, force is obtained by using (4).

C. Results

Figure 12 shows the step response for the vertical direction, motion of rotor. In this figure we present both fitted linear and nonlinear models versus experimental data. As we can see the simulation results are quite acceptable.

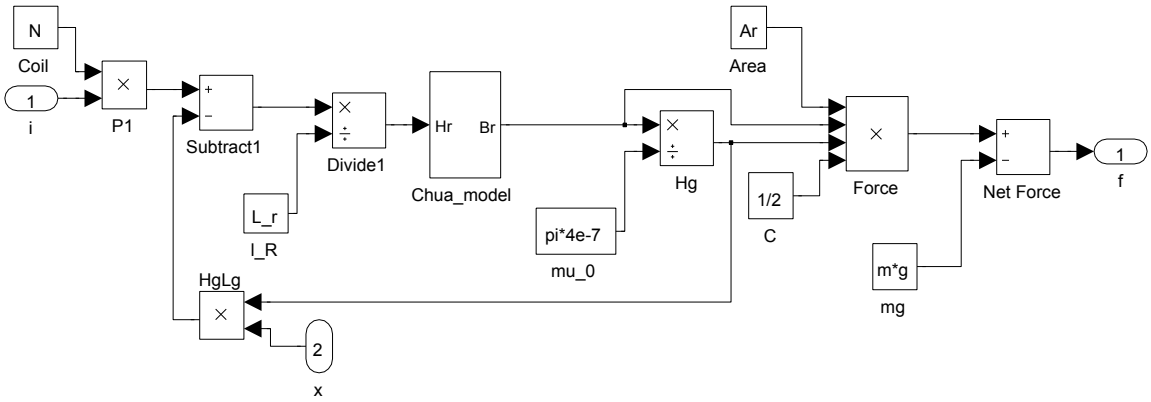

Fig. 10. Force generation in nonlinear bearing model including Chua hysteresis model.

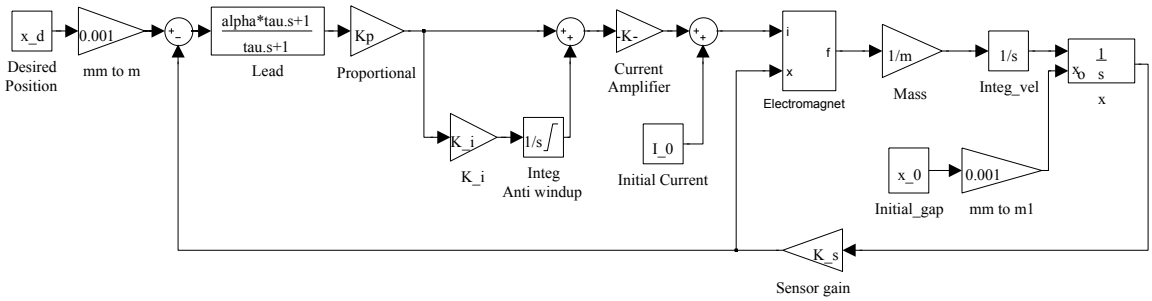

Fig. 11. Hysteresis self-bearing suspension control block diagram. Nonlinear force model is enclosed in block labeled Electromagnet.

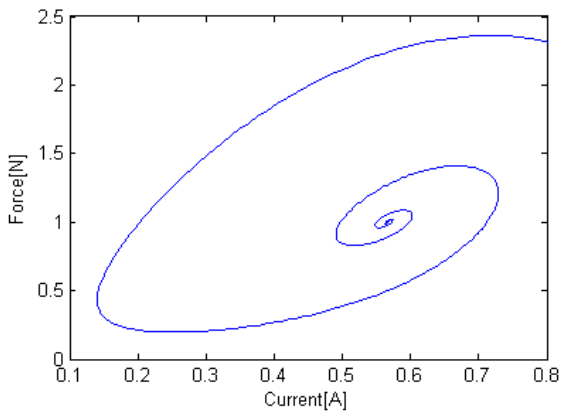

Fig. 13. Force v.s. Current during transition of an 0.1mm step input from initial 0.5mm gap.

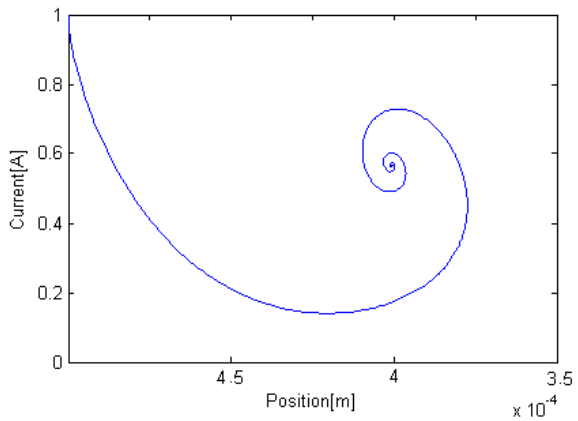

Fig. 14. Current v.s. Displacement during transition of an 0.1mm step input from initial 0.5mm gap.

Figures 13 and 14 shows the force versus current and current versus displacement during the step transition. These simulations are run for a gap=0.5mm and a step of 0.1mm.

Figure 15 shows the B-H trajectory in the rotor during a step transition.

The motor torque analysis is also calculated and presented in [6]. Figure 16 shows the rotor speed versus time for both model and experimental results. Figure 17 shows the hunting phenomenon that was measured experimentally at 2100 rpm. As we can see, it takes about 1 minute for the oscillation to die. This is because we didn't actively control the speed; however if hunting is an issue for a particular application it can be easily resolved by speed control.

IV. Conclusion

In this paper, a novel self-bearing motor has been proposed. A segmented stator hysteresis self-bearing motor was designed and tested successfully. FEA simulation was done to check the

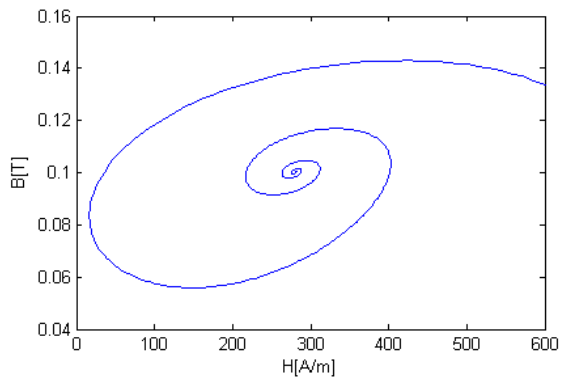

Fig. 15. Plant B-H during transition of an 0.1mm step input from an initial 0.5mm gap.

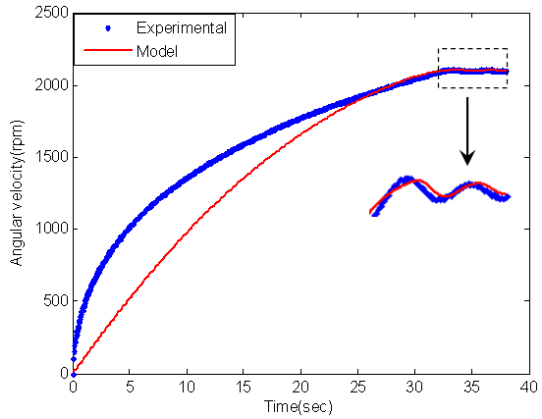

Fig. 16. Speed vs time under 0.5 A rms excitation. Blue curve is experiment and red curve is model.

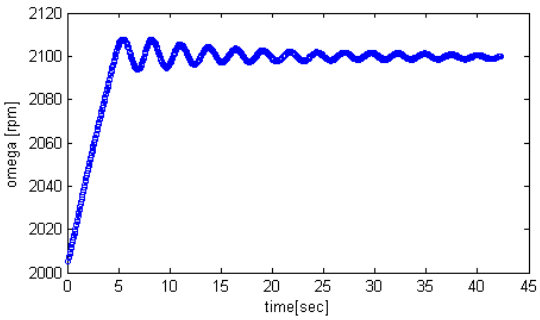

Fig. 17. Measured speed hunting at 2100 rpm.

feasibility of such a system. Later a nonlinear analysis based on Chua model is provided to simulate the system behavior.

V. Acknowledgment

The authors would like to thank the MIT Energy Initiative for funding this project.

References

[1] A. Chiba, D. T. Power and M. A. Rahman, "Charachteristic of a bearingless induction motor," *IEEE Trans. Magn.*, Vol.27, no.6, pp 5199-5201,Nov. 1991.

[2] R. Schoeb and J. Bischel, "Vector control of the bearingless motor," in *Proc. 4th ISMB*, Zurich, Switzerland, pp 327-332,1994.

[3] J. J. Nitao, E. T. Scharlemann and B. A. Kirkendal, "Equivalent circuit modeling of hysteresis motors," in *Techincal report, Lawrence Livermore National Laboratory*,2009.

[4] L. O. Chua and K. A.. Stromsmoe, "Lumped circuit model for nonlinear inductors exhibiting hysteresis loops," *IEEE Trans. Circuit Therory.*,.1970.

[5] L. O. Chua and S. C.. Bass, "A generalized hysteresis model," *IEEE Trans. Circuit Therory.*, Vol.19, no.1, pp 36-48,Nov. 1972.

[6] M. Imani Nejad and D. L.. Trumper, "Self-bearing motor design and control," *PhD Thesis.*, Mechanical Engineering, MIT,. Cambridge. 2013.